Drebrin regulates cytoskeleton dynamics in migrating neurons through interaction with CXCR4

Yufei Shan[a], Stephen Matthew Farmer[a], and Susan Wray[a,1]

[a]Cellular and Developmental Neurobiology Section, National Institute of Neurological Disorders and Stroke, National Institutes of Health, Bethesda, MD 20892

Edited by Pasko Rakic, Yale University, New Haven, CT, and approved December 3, 2020 (received for review May 14, 2020)

Stromal cell-derived factor-1 (SDF-1) and chemokine receptor type 4 (CXCR4) are regulators of neuronal migration (e.g., GnRH neurons, cortical neurons, and hippocampal granule cells). However, how SDF-1/CXCR4 alters cytoskeletal components remains unclear. Developmentally regulated brain protein (drebrin) stabilizes actin polymerization, interacts with microtubule plus ends, and has been proposed to directly interact with CXCR4 in T cells. The current study examined, in mice, whether CXCR4 under SDF-1 stimulation interacts with drebrin to facilitate neuronal migration. Bioinformatic prediction of protein–protein interaction highlighted binding sites between drebrin and crystallized CXCR4. In migrating GnRH neurons, drebrin, CXCR4, and the microtubule plus-end binding protein EB1 were localized close to the cell membrane. Coimmunoprecipitation (co-IP) confirmed a direct interaction between drebrin and CXCR4 using wild-type E14.5 whole head and a GnRH cell line. Analysis of drebrin knockout (*DBN1* KO) mice showed delayed migration of GnRH cells into the brain. A decrease in hippocampal granule cells was also detected, and co-IP confirmed a direct interaction between drebrin and CXCR4 in PN4 hippocampi. Migration assays on primary neurons established that inhibiting drebrin (either pharmacologically or using cells from *DBN1* KO mice) prevented the effects of SDF-1 on neuronal movement. Bioinformatic prediction then identified binding sites between drebrin and the microtubule plus end protein, EB1, and super-resolution microscopy revealed decreased EB1 and drebrin coexpression after drebrin inhibition. Together, these data show a mechanism by which a chemokine, via a membrane receptor, communicates with the intracellular cytoskeleton in migrating neurons during central nervous system development.

neuronal migration | drebrin | CXCR4 | GnRH | hippocampus

Proper neuronal migration is essential for neural circuits formation (1) and requires coordination of extracellular signals and intracellular processes that results in cytoskeletal changes. Several modes of neuronal migration have been characterized, but all must transduce extracellular signals into appropriate movement. For bipolar migrating neurons (cerebellar granule cells (2, 3), cortical pyramidal cells (4), and neuroendocrine gonadotropin releasing hormone (GnRH) cells (5), the leading process extends toward a target, and the pulling forces of microtubule bundles anchored to the thin layer of cortical actin via end-binding proteins moves the nucleus forward. This process is sequentially repeated as the neuron migrates toward its final location (6–8). Although the basic dynamics of cell movement are being delineated, how a neuron ends up in the correct location, integrating extracellular guidance cues into cytoskeletal modifications, is still unclear.

The stromal cell–derived factor-1 (SDF-1)/C-X-C chemokine receptor type 4 (CXCR4) chemotactic axis is directly involved in migration of hippocampal (9, 10), cortical (4, 11), cerebellar (2, 12–14), and GnRH cells (15–17). Research in T lymphocytes documented SDF-1–induced cytoskeletal alterations, where rapid actin dynamics occur during formation of immune synapses (18). Developmentally regulated brain protein (drebrin), an actin filament side-binding protein that stabilizes the double-strained F-actin structure, was colocalized with the CXCR4 receptor cytoplasmic domain in these immune synapses. A physical interaction between CXCR4 and drebrin via coimmunoprecipitation (co-IP) was shown, suggesting that after SDF-1 activation, CXCR4 directly regulated cytoskeletal components by binding to drebrin. The function of drebrin in migrating neurons has only been analyzed in the rostral migratory stream, cerebellar granule neurons, and oculomotor neurons in mice. In these areas, *Drebrin short hairpin RNA* reduced the migration distance and velocity of migrating neurons (19–21).

In contrast to drebrin, multiple studies have documented changes in neuronal migration after SDF-1/CXCR4 perturbations. SDF-1/CXCR4 has been shown to act as a chemoattractant for cerebellar granule cell progenitor migration and Purkinje neuron migration (2, 12), while in the developing cerebral cortex, it regulates interneuron migration (4, 11). In the hippocampus, meningeal/Cajal–Retzuis cells secrete SDF-1 (22). Here, the SDF-1 gradient is important for radial migration in the dentate gyrus (DG), specifically granule cells. CXCR4 mutant mice have a defect in granule cell position, while ectopic expression of SDF-1 disrupted DG granule cell migration (9). In addition, blocking SDF-1/CXCR4 signaling resulted in precocious differentiation, delayed migration, and ectopic granule cell progenitors (23). SDF-1/CXCR4 has also been well studied in the developing GnRH system. Neuroendocrine GnRH neurons migrate from the olfactory pit into the forebrain (5). The primary source of SDF-1 for GnRH neuronal migration are cells located close to the nasal midline cartilage, just beneath the cribriform plate (17). These cells create a gradient of SDF-1 that guides the GnRH neurons to the nasal/forebrain junction. Silencing of CXCR4 results in fewer GnRH neurons reaching the nasal

Significance

Proper neuronal migration is critical for the formation of correct neural circuits during development. Chemokines are known to facilitate neuronal migration. However, the underlying mechanism is still unclear. Here, we reveal a novel mechanism whereby the chemokine receptor (CXCR4), after being activated by its ligand, SDF-1, interacts directly with the cytoskeleton compartment via drebrin, an actin-binding protein that interacts with microtubule plus-end–binding proteins. The interaction between activated CXCR4/drebrin promotes neuronal migration. The study provides insights on the relationship between extracellular cues and intracellular components.

Author contributions: Y.S. and S.W. designed research; Y.S. and S.M.F. performed research; Y.S., S.M.F., and S.W. analyzed data; and Y.S., S.M.F., and S.W. wrote the paper.

The authors declare no competing interest.

This article is a PNAS Direct Submission.

[1]To whom correspondence may be addressed. Email: wrays@ninds.nih.gov.

This article contains supporting information online at https://www.pnas.org/lookup/suppl/doi:10.1073/pnas.2009493118/-/DCSupplemental.

Published January 7, 2021.

forebrain junction (15, 16), while application of SDF-1 augments GnRH saltatory movement (17), a moving pattern similar to radial migrating neurons (24). Although CXCR4 on the plasma membrane has been shown to be internalized upon ligand binding (23), how SDF-1/CXCR4 regulates cytoskeleton dynamics in neurons is still unclear.

The present study examined the interaction of drebrin and CXCR4 in migrating neurons. Bioinformatic analysis predicted a protein–protein interaction between drebrin and CXCR4. Co-IP confirmed a direct interaction between drebrin and CXCR4 in GnRH cells and in hippocampal areas. Analysis of drebrin knockout (*DBN1* KO) mice showed delayed migration of GnRH cells into the brain and disrupted organization of granule cells in the hippocampus. Migration assays on primary GnRH cells, as well as modified Boyden chamber assays on primary DG granule cells, established that inhibiting drebrin (either pharmacologically or using cells from *DBN1* KO mice) prevented the effects of SDF-1/CXCR4 on neuronal movement. Bioinformatic prediction then was used to identify potential binding sites between drebrin and the microtubule plus end protein EB1, and super-resolution microscopy revealed decreased EB1 and drebrin coexpression after drebrin or CXCR4 inhibition. Together, these data show a mechanism by which a chemokine, via a membrane receptor, communicates with the intracellular cytoskeleton in migrating neurons during early central nervous system (CNS) development.

Results

Theoretical Prediction of Physical Interaction between Drebrin and CXCR4 Confirmed by Co-IP. Domain-specific functional studies of drebrin have revealed binding regions for F-actin and CXCR4 (18, 25–27). However, structural analyses have not been conducted on drebrin/CXCR4 interactive binding. SwarmDock and PatchDock were used to predict a potential binding pose (*SI Appendix*, *Supplemental Methods*). Simulations revealed that drebrin can potentially stabilize with CXCR4 in four areas: a drebrin coiled-coil (CC) domain forming a convex binding arm with two CXCR4 intracellular loops (ICLs) where 1) CC (R215/E202) binds to ICL1 (K68/R70), 2) CC (L204/D201) binds to ICL2 (Q145/R148), 3) a drebrin actin-depolymerizing factor homology (ADFH) domain forming a concave binding arm (D92) with CXCR4's ICL3 (K239), and 4) a drebrin helical (Hel) and ADFH domains forming a hydrophobic shell (residues 112 to 119 and 283 to 291) to insert CXCR4's C-terminal tail (Fig. 1*A*). Predicting the biological interface and affinity between these proteins is beneficial to confirm overall stabilization of the complex. PRODIGY predicted that drebrin/CXCR4 binding consists of charged (60%), apolar-apolar (20%), and polar-apolar/polar-polar (20%) bond distribution. To further validate the predicted charged interactions, artificial alanine (A) mutations were introduced in drebrin. Although CXCR4 bound to the artificial drebrin mutant (R215A, E202A, L204A, D201A, and D92A) had a slightly more favorable binding free energy ($\Delta G_{drebrin(mut)/CXCR4} = -10.7$ kcal $\cdot$ mol^{-1}) compared to wild-type (WT) drebrin ($\Delta G_{drebrin(wt)/CXCR4} = -10.5$ kcal $\cdot$ mol^{-1}), there was an overall decrease in charged–charged (−28%) and charged–polar (−26%) bonds at the binding interface. These data are consistent with these sites being involved in CXCR4/drebrin binding, but further molecular experiments are needed to precisely delineate this interaction.

Experimental confirmation of a drebrin/CXCR4 interaction was obtained on E14.5 mouse head protein via co-IP using an N-terminal–directed CXCR4 antibody and C-terminal–directed drebrin antibody (Fig. 1*B*). The pull-down (PD) products and the flowthrough (FT) samples were assayed via Western blot, incubated with anti-CXCR4 and anti-drebrin antibody, with the order depending on the antibody linked to the magnetic beads. Both drebrin (125 kDa) and CXCR4 (60 kDa) were detected in control protein samples (Fig. 1*B*, whole lysate [WL], as well as the FT). The pull-down elution from anti-drebrin–conjugated beads yielded drebrin bands, confirming the efficacy of the co-IP procedure (Fig. 1*B*, immunoblotting target [IB]: drebrin). Notably, CXCR4 bands were also detected in the pull-down samples, confirming a physical interaction between drebrin and CXCR4 (Fig. 1*B*, IB: CXCR4). The reverse pull-down experiments confirmed the association between drebrin and CXCR4 (i.e., beads conjugated with anti-CXCR4 gave positive bands for drebrin). Another GPCR, cholecystokinin A receptor (CCKA), known to be expressed on migrating GnRH cells (28) was used as a negative control in Western blot with co-IP pull-down products. CCKA was detected in WL and FT samples (45 kDa, Fig. 1*B*, IB: CCKA). However, no CCKA band was detected in the pull-down product (IB: CCKA, PD lane), consistent with the binding of drebrin/CXCR4 being specific and not a general GPCR phenomenon.

Drebrin and CXCR4 Interaction in Migrating GnRH Neurons. To begin to evaluate the biological role of the CXCR4/drebrin interaction, drebrin and CXCR4 in GnRH neurons, known to be guided by SDF-1/CXCR4, were examined. At E12.5 (Fig. 1 *C*–*E*), a developmental time point when many GnRH neurons are migrating toward the forebrain (Fig. 1*C*) (29), drebrin and CXCR4 were detected along the cortical actin in the leading process and cell soma (Fig. 1*D*, arrowheads), showing overlapping distribution patterns (Fig. 1*D*, merged, orthogonal profile). For a neuron to migrate properly, the anchoring of microtubule plus ends into cortical actin mesh is necessary to facilitate a forward pulling force (30). The microtubule plus-end binding protein EB1, detected in migrating GnRH cells (31), localized in both soma (Fig. 1*E*, bottom asterisk) and leading processes (Fig. 1*E*, top asterisk) in GnRH cells, similar to drebrin (Fig. 1*D*). Next, protein from a GnRH cell line were assayed by co-IP as described above, and the pull-down products and the flow through samples assayed via Western blot (*SI Appendix*, Fig. S1). Consistent with results obtained on E14.5 head protein, CXCR4 bands were detected in the anti-drebrin pull-down samples (IP: drebrin, PD lane), drebrin bands were detected in the anti-CXCR4 pull-down samples (IP:CXCR4, PD lane), and no CCKA band was detected (IB: CCKA, PD lane). Together, these data indicate that drebrin and CXCR4 can directly interact in migrating neurons.

Delayed Migration of GnRH Cells and Decreased Neurons in the Hippocampal Granule Cell Layer in *DBN1* KO Mice. Although brain morphometric data had shown no gross changes in *DBN1* KO animals (*SI Appendix*, Table S1), two systems known to be sensitive to CXCR4, the GnRH system and DG granule cells in the hippocampus were examined in *DBN1* KO and WT littermates. The total GnRH cell number and anatomical distribution of the cells was analyzed (Fig. 2*A*). At E12.5, *DBN1* KO animals had significantly less GnRH-positive neurons compared to WT littermates ($P = 0.0481$). χ^2 analysis indicated a significant difference in the distribution of GnRH cells between genotypes ($P < 0.0001$), and individual area comparisons indicated fewer GnRH neurons at the nasal forebrain junction in E12.5 KO mice ($P = 0.0409$). At both postnatal day 4 (PN4) and adult, the total GnRH cell number counted in *DBN1* KO and WT were similar. However, χ^2 analysis indicated a significant difference in the distribution of GnRH cells in genotypes at both ages ($P < 0.0001$), and individual area comparisons indicated more GnRH neurons were rostral to the organulum vasculosum lamina terminalis (OVLT) in both PN4 and adult KO mice (PN4 $P = 0.0058$, adult $P = 0.0173$).

Since SDF-1/CXCR4 is robustly expressed in the developing hippocampal area between PN0 and PN8 (32), the DG of PN4 (Fig. 2*B*) and adult (*SI Appendix*, Fig. S2) *DBN1* KO and WT

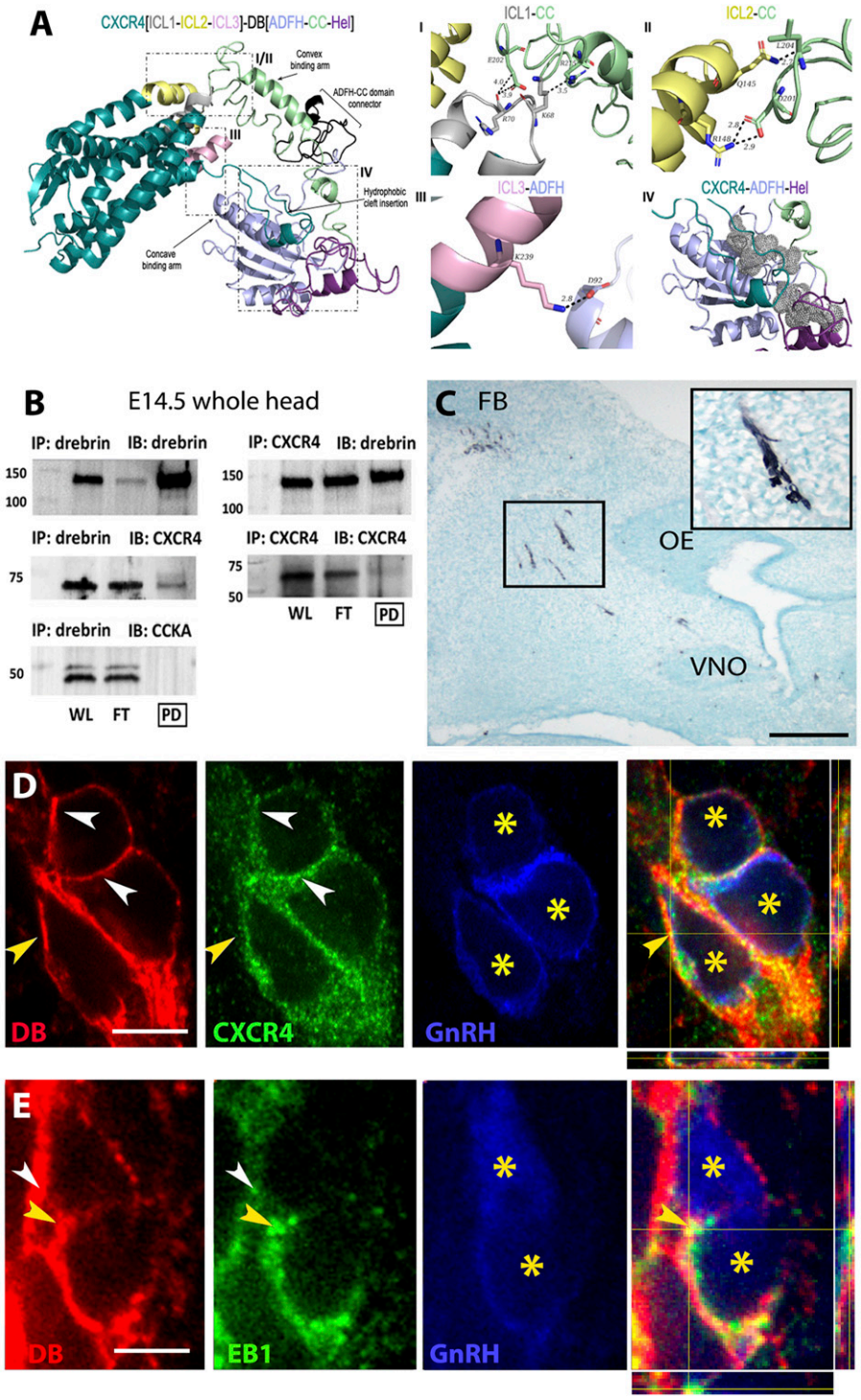

Fig. 1. Drebrin and CXCR4 physically interacted in migrating GnRH neurons. (*A*) Intracellular docking between crystallized CXCR4 (Protein Data Bank: 3ODU) and drebrin N-terminal domains. Low magnification (*Left*) and higher magnification (*Right*) shown of four possible interacting domains: 1) CXCR4's ICL1 (K68/R70) bound to drebrin's CC (R215/E202), 2) CXCR4's ICL2 (Q145/R148) bound to drebrin's CC (L204/D201), 3) CXCR4's ICL3 (K239) bound to drebrin's ADFH (D92), and 4) hydrophobic coat created by drebrin's ADFH and Hel domains (residues 112 to 119 and 283 to 291) that wraps around CXCR4's C-terminal tail. (*B*) Representative pull-down experiments using anti-drebrin (IP: drebrin) or anti-CXCR4 (IP: CXCR4) from E14.5 mouse whole head. IP: immunoprecipitation target, IB: immunoblotting target, WL: whole lysate, FT: flow through. Visible CXCR4 (IB: CXCR4, 60 kDa) and drebrin (IB: drebrin, 125 kDa) bands were detected in pull-down (PD) lanes. (*C*) Migrating GnRH neurons detected in E12.5 mouse embryo. High-magnification GnRH-positive neurons are shown (*Inset*). FB: forebrain, OE: olfactory epithelium, VNO: vomeronasal organ. (Scale bar, 100 μm.) (*D*) Confocal immunofluorescent staining of drebrin (red) and CXCR4 (green) localized in migrating GnRH neurons (blue, asterisks) in vivo at E12.5. Colocalization was detected at cytoplasmic membrane region as well as leading processes (white and yellow arrow heads). (*E*) Drebrin (red) and EB1 (green) colocalization detected in GnRH neurons (blue, asterisks) at both somatic membrane and leading processes (white and yellow arrow heads). Merged images in the fourth panels of *D* and *E* show colocalized puncta (yellow arrows) in a single z-plane. (Scale bars in *D* and *E*, 10 μm.)

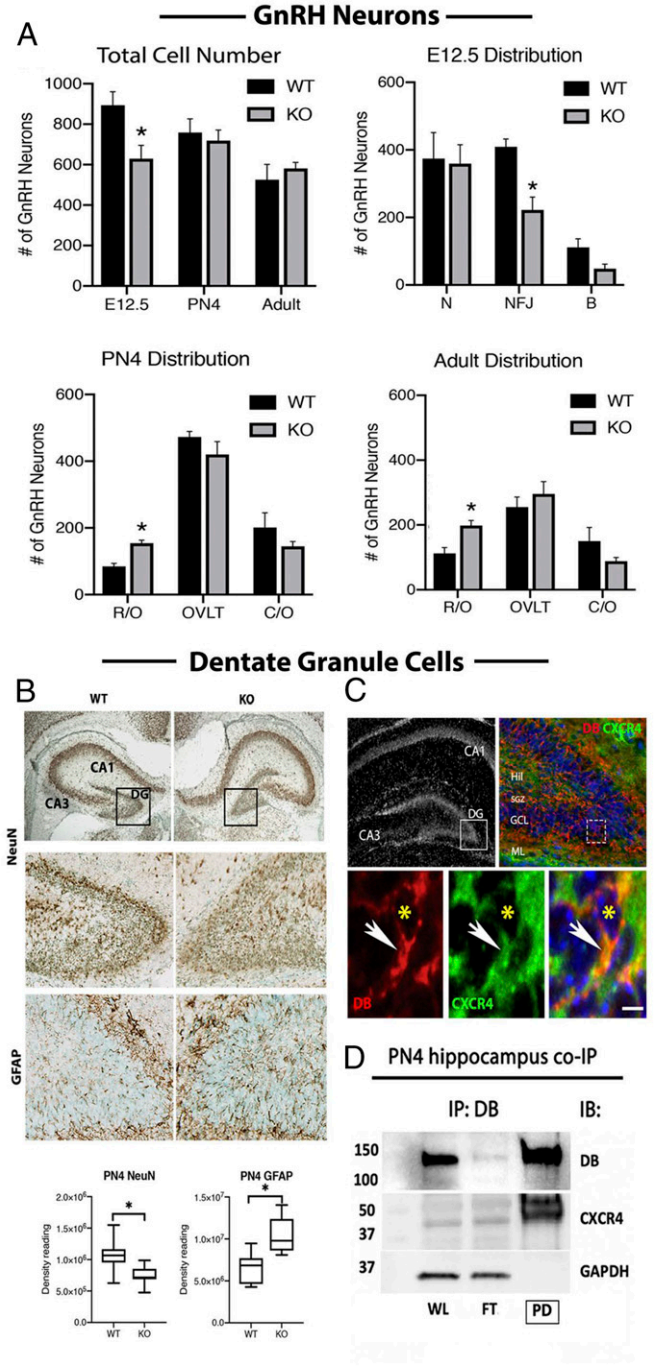

Fig. 2. Lack of drebrin-delayed GnRH neuronal migration and decreased DG granule cells. (*A*) Significantly fewer GnRH cells were observed in *DBN1* KO animals at E12.5 ($n = 3$ WT and 3 KO; $^*P = 0.0481$, unpaired t test). The distribution of GnRH cells plotted at ages E12.5, PN4, and adulthood is shown. χ^2 analysis of the distribution of GnRH cells at each age revealed a significant difference between WT and KO mice ($^*P < 0.0001$ for each age). At E12.5, *DBN1* KO mice had less GnRH cells than WT controls at the NFJ ($^*P = 0.0409$, unpaired t test), accounting for the overall decrease detected in the total GnRH cell number. No differences were detected in either the nasal region or brain, consistent with a delay in GnRH cell development. In both PN4 and adult mice, *DBN1* KO had more GnRH cells rostral to the OVLT as compared to controls (PN4, $^*P = 0.0173$; adult, $^*P = 0.0216$; unpaired t test), consistent with an overall delay in migration that cannot compensate with time. NFJ: nasal forebrain junction, B: brain, R/O: rostral to OVLT, C/O: caudal to OVLT. (*B*) WT (*Left*) and KO (*Right*) PN4 hippocampi were stained for NeuN and GFAP. The intensity of NeuN and GFAP was plotted and compared between genotypes ($n = 3$, unpaired t test). A significant decrease was found in cells stained for NeuN, while a significant increase was detected in overall GFAP staining. (*C*) Immunocytochemistry revealed colocalization of drebrin (red) and CXCR4 (green) in a migrating hippocampal granule cell at PN4 (white arrow, asterisks). Hil: hillius, GCL: granule cell layer, ML: molecular layer. (Scale bar, 10 μm.) (*D*) Drebrin immunoprecipitation from PN4 hippocampal protein sample detected CXCR4 bands in pull-down product. Drebrin immunopositive bands are shown at 125 kDa. GAPDH was used for negative control, and no band was detected in the PD lane. IP: immunoprecipitation target, IB: immunoblotting target, WL: whole lysate, FT: flow through, PD: pull-down.

mice were also examined. At both ages, a reduction was found in NeuN staining density while an increase was measured in glial fibrillary acidic protein (GFAP) staining in *DBN1* KO mice. No difference was found in the number of Sox2 positive cells (a marker for multipotent neural stem cells) in the adult subgranular zone (SGZ), the region of the hippocampus where adult neurogenesis occurs (33) (*SI Appendix*, Fig. S3). Using PN4 hippocampal tissue, immunofluorescence staining verified that drebrin and CXCR4 colocalized in cells in the DG granule cell layer (Fig. 2*C*), and co-IP confirmed an interaction between drebrin and CXCR4 (Fig. 2*D*). Taken together, these results from *DBN1* KO mice are consistent with drebrin/CXCR4 interactions modulating GnRH neuronal migration as well as hippocampal granule cell layer development in vivo.

Functional Migration Assays Indicate Drebrin Inhibition Attenuates SDF-1/CXCR4–Induced Movement in GnRH Cells and DG Granule Cells. To directly test whether drebrin and CXCR4, acting together, alter neuronal movement, experiments were performed on primary GnRH cells maintained in embryonic nasal explants and DG granule cells cultured on transwell inserts (Fig. 3). Nasal explants are a well-described model system in which one can monitor GnRH cell migration (34). Fluorescent immunostaining indicated drebrin, CXCR4, and EB1 were expressed in GnRH neurons maintained in explants along the cortical actin (Fig. 3 *A–C*) in both the soma (arrow) and in the leading processes (arrow heads). Thus, the in vitro pattern mimicked the in vivo pattern (compare Fig. 3 *A–C* to Fig. 1 *D* and *E*). Notably, using nasal explants, one can manipulate the concentration of SDF-1 by making unilateral explants that remove midline SDF-1 producing cells (Fig. 3 *D* and *E*) (17). In bilateral explants, the migration rate of GnRH neurons was slower in cells from *DBN1* KO mice compared to WT (Fig. 3 *D* and *F*), consistent with the in vivo data, indicating a slower GnRH migratory rate (Fig. 2*A*). However, in unilateral explants (lower SDF-1 levels), the migration rate of GnRH neurons was similar in explants generated from WT and *DBN1* KO mice (Fig. 3*E*). As shown previously (17), application of exogenous SDF-1 to unilateral explants derived from WT mice increased the migration rate of GnRH neurons (Fig. 3 *E* and *G*, WT + SDF versus WT). In contrast, exogenous SDF-1 did not alter the migration rate of GnRH neurons in unilateral explants derived from *DBN1* KO mice (Fig. 3*E*, KO + SDF versus KO). WT and *DBN1* KO explants were stained for CXCR4 and GnRH. CXCR4 was less abundant in the leading processes of GnRH neurons in *DBN1* KO compared to WT littermates (Fig. 3 *H–J*). A second set of migration experiments was performed on isolated DG granule cells using modified Boyden chamber assays (Fig. 3*K*). Addition of hepatocyte growth factor (HGF) (28) in the lower compartment increased migration of granule cells derived from both WT and *DBN1* KO mice (Fig. 3*L*). Like HGF, addition of SDF-1 in the lower chamber resulted in increased migration of granule cells derived from WT mice into the lower compartment. In contrast, addition of SDF-1 in the lower chamber did not attract more granule cells derived from *DBN1* KO mice to move across the membrane (Fig. 3*L*). Together, these data show a functional

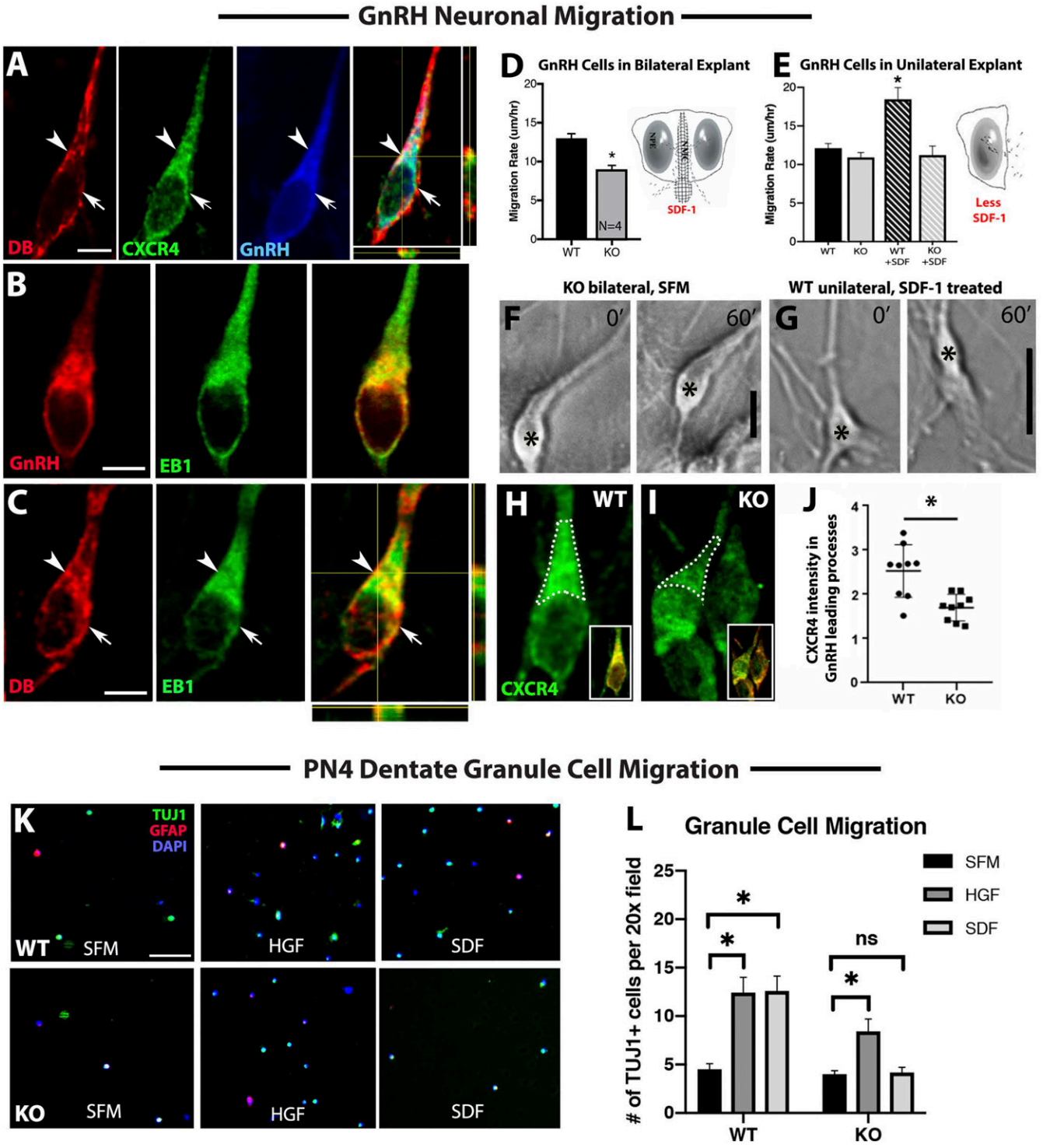

Fig. 3. Primary neurons from *DBN1* KO mice do not respond to SDF-1 stimulation. (*A*–*C*) Immunocytochemistry on primary GnRH neurons (blue) maintained in explants showed coexpression of drebrin (red) and CXCR4 (green) and drebrin (red) and EB1 (green). Expression was seen in the leading process (arrow heads) and soma (arrows) of migrating GnRH neurons. Merged images in the third panel of *A* and *C* show colocalized puncta (arrow heads) in a single z-plane. (*D*–*G*) Histogram shows primary GnRH neurons derived from *DBN1* KO mice migrate slower than WT littermates in bilateral condition, when explants contain endogenous SDF-1 (*D* and *F*, N = 4, $^*P < 0.0001$ unpaired *t* test). However, the WT/KO difference was eliminated in unilateral explants with lower amounts of endogenous SDF-1, and exogenous SDF-1 rescue was not detected in GnRH cells from KO mice (*E* and *G* for WT/KO, N = 4, $P = 0.16$, unpaired *t* test; for WT/WT-SDF and KO/KO-SDF, paired *t* test, N = 4; WT $n = 49$, $^*P < 0.0001$; KO $n = 50$, $P = 0.8075$). Black bars in *F* and *G* indicate linear migration distances from 0′ to 60′. The asterisks indicate the location of the cell nuclei. (*H*–*J*) Optical density analysis of immunofluorescence in the leading process of GnRH neurons (dotted lines in *H* and *I*) showed reduced CXCR4 expression (green) in cells from *DBN1* KO mice compared to cells from WT controls. The insets in *H* and *I* show a lower magnification, merged image of cells in double labeled for GnRH (yellow) and CXCR4 (green). (*K* and *L*) Modified Boyden chamber assays showed that DG granule cells obtained from *DBN1* KO mice respond to HGF but do not respond to SDF. Representative images of each group are shown in *K* (TUJ1, green; GFAP, red; Dapi, blue). Data are shown in histograms (*L*) (unpaired *t* test, N = 3 [pairs of litters], $n = 4$ [20× fields per treatment group/genotype], $^*P < 0.05$, ns, not significant). (Scale bars, [*A*–*C*] 10 μm and [*K*] 50 μm.)

correlation between SDF-1/CXCR4 signaling and drebrin in migrating neurons.

Pharmacological blockade of drebrin mimics DBN1 KO. BTP2 is a cell-permeable pyrazole that has been implicated as a blocker of Stim1 and Orai1-coupled Ca^{2+} release-activated Ca^{2+} (CRAC) channel-mediated store-operated Ca^{2+} entry [SOCE, (35)]. However, Mercer et al. (36) reported that BTP2 acts on CRAC channels by inhibiting drebrin, confirmed via BTP affinity probes, pull-down assays, and protein mass spectroscopic analyses. Thus, a series of experiments was performed in which BTP2 was applied to GnRH neurons maintained in bilateral and unilateral explants from WT mice and GnRH neuronal migration rate was measured and values compared to control periods (Fig. 4). In the presence of endogenous SDF-1 (bilateral explant), application of BTP2 significantly reduced GnRH neuronal migration rate compared to the serum-free media (SFM) control period (33% reduction, Fig. 4*A*). These bilateral explants from WT mice (Fig. 4*A*) were stained for CXCR4 and GnRH (Fig. 4*E*). CXCR4 staining appeared attenuated in the leading processes of BTP2-treated GnRH neurons (black arrows) compared to WT littermates (white arrows) and similar to that detected in explants generated from *DBN1* KO mice (Fig. 3*I*). To ensure that the action of BTP2 was not via CRAC channel–regulated Ca^{2+} influx, Synta66 (a CRAC channel–specific blocker) (37) was applied before BTP2. Synta66 treatment attenuated the rate of GnRH neuronal migration. However, upon application of BTP2, a further reduction (−22%) in GnRH neuronal migration rate occurred (Fig. 4*B*). Notably, a decrease in cell migration rate was not detected when BTP2 was omitted during the third period, following Synta66 treatment during the second period (SFM first period = 14.14 ± 0.66, Synta66 second period = 10.83 ± 0.76, Synta66 third period = 13.46 ± 0.76, N = 3, n = 60), indicating that the decreased migration rate with BTP2 treatment in the third period was not due to residual Synta66 effects (i.e., blockade of CRAC channels). Thus, the change in GnRH neuronal migration rate after application of BTP2 is consistent with BTP2-inhibiting drebrin.

Specificity of drebrin/CXCR4 functional interaction. To further verify that the BTP2 was specifically blocking the drebrin interaction with CXCR4, two other receptors known to modulate GnRH neuronal migration when activated, were examined in the presence of BTP2: $GABA_AR$ (17) and GPR37 (38). Inhibition of $GABA_AR$ and activation of GPR37 have been shown to increase the GnRH neuronal migration rate. Both the $GABA_AR$ inhibitor picrotoxin (PIC) and the GPR37 agonist TX-14 increased the migration rate in the presence of BTP2 (Fig. 4 *C* and *D*). Next, a series of experiments was performed in unilateral explants from WT mice (Fig. 5). BTP2 treatment blocked the increase seen in the cell migration rate upon the addition of SDF-1 (Fig. 5 *A* and *B*) but not upon addition of TX-14 (Fig. 5*C*). CRAC channel blockers should impair signaling of GPCRs that work via activation of phospholipase C (PLC) (39, 40). GPR37 has been proposed to act via this pathway (41). Thus, in two independent experimental groups, the PLC blocker, U73122, or Synta66 was applied to explants, followed by the GPR37 agonist TX-14. In contrast to BTP2 application, no significant increase in the neuronal migration rate was detected in either group after TX-14 application, proving that the signaling pathway downstream of GPR37 1) activates PLC and 2) is sensitive to Synta66 (PLC inhibition; SFM = 13.47 ± 0.63, U73122 = 15.69 ± 1.337, TX-14 = 12.33 ± 0.95, N = 3, n = 59, P = 0.28; Synta66, see Fig. 5*D*). Together, these data are consistent with the action of BTP2 being independent of CRAC channel–regulated Ca^{2+} influx and support the specificity of BTP2 at blocking drebrin and, subsequently, the function of SDF-1/CXCR4 signaling. The increase in GnRH neuronal migration via SDF-1 stimulation was also shown to be dependent on activation of G protein–coupled inward rectifier K^+ (GIRK) channels (17). However, no further increase of the migration rate was observed in either *DBN1* KO (Fig. 3*E*) or BTP2-pretreated (Fig. 5*B*) unilateral explants with exogenous application of SDF-1, suggesting that GIRK activation via SDF-1 could not override the loss of drebrin to produce cell movement. A set of BTP2 experiments was then performed on cultured DG granule cells using modified Boyden chamber assays. Application of BTP2 did not alter the HGF chemokine effect; however, it abolished the effect of SDF-1 (Fig. 5 *E* and *F*), similar to that observed in DG granule cells derived from *DBN1* KO mice (Fig. 3*L*).

Inhibiting Drebrin Interrupts Capturing of EB1 at Cortical Actin Mesh. EB1 is a microtubule plus-end protein that guides microtubule plus ends into cortical actin to facilitate neuronal migration (42). Using a similar experiment-informed approach to determine docking, we predicted EB1 to use a posthelix extension to latch itself onto a hydrophobic pit created by drebrin residues 404 through 424 which intersects drebrin's polyproline (PP) and blue-box disordered (BB) domains (Fig. 6*A*). Hydrophobic

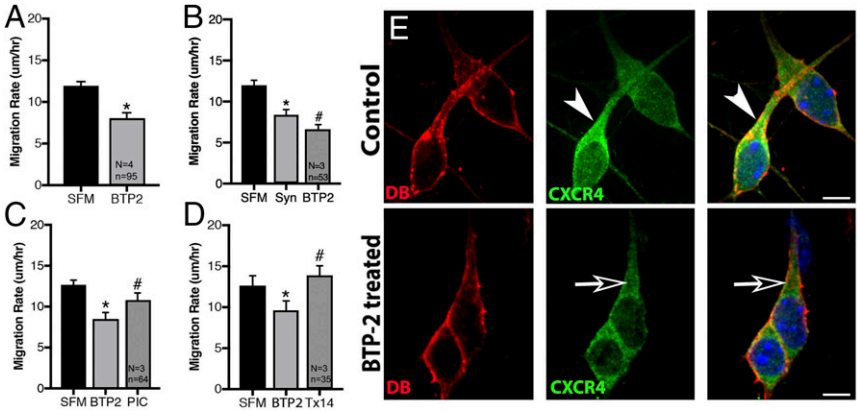

Fig. 4. Pharmacological blockade of drebrin attenuated GnRH migration in bilateral explants with endogenous SDF-1. (*A*) In bilateral explants, the drebrin inhibitor BTP2 decreased GnRH migration rate (N = 4, n = 95, $^*P < 0.0001$, paired t test). (*B*) BTP2 decreased GnRH migration rate after treatment with the CRAC channel–specific blocker Synta66 (Syn) application (N = 3, n = 53, $^*P < 0.0001$, $^{\#}P = 0.0093$, paired t test). (*C* and *D*) BTP2 application did not block the increase in migration rate associated with blockade of $GABA_AR$ via PIC (17) or GPR37 activation via TX-14 (38). (*C*) N = 3, n = 64, $^*P < 0.0001$, $^{\#}P = 0.0114$; (*D*) N = 3, n = 35, $^*P = 0.0453$, $^{\#}P = 0.0070$, paired t test. (*E*) Immunocytochemistry showed that in both BTP2-treated and control explants, drebrin (red) is expressed in a similar pattern in the GnRH cell soma and leading process, being found along the cortical actin. However, in BTP2-treated explants, GnRH neurons showed attenuated CXCR4 expression (green, black arrows) in the leading processes compared to cells in control explants (white arrow heads). (Scale bar, 10 μm.)

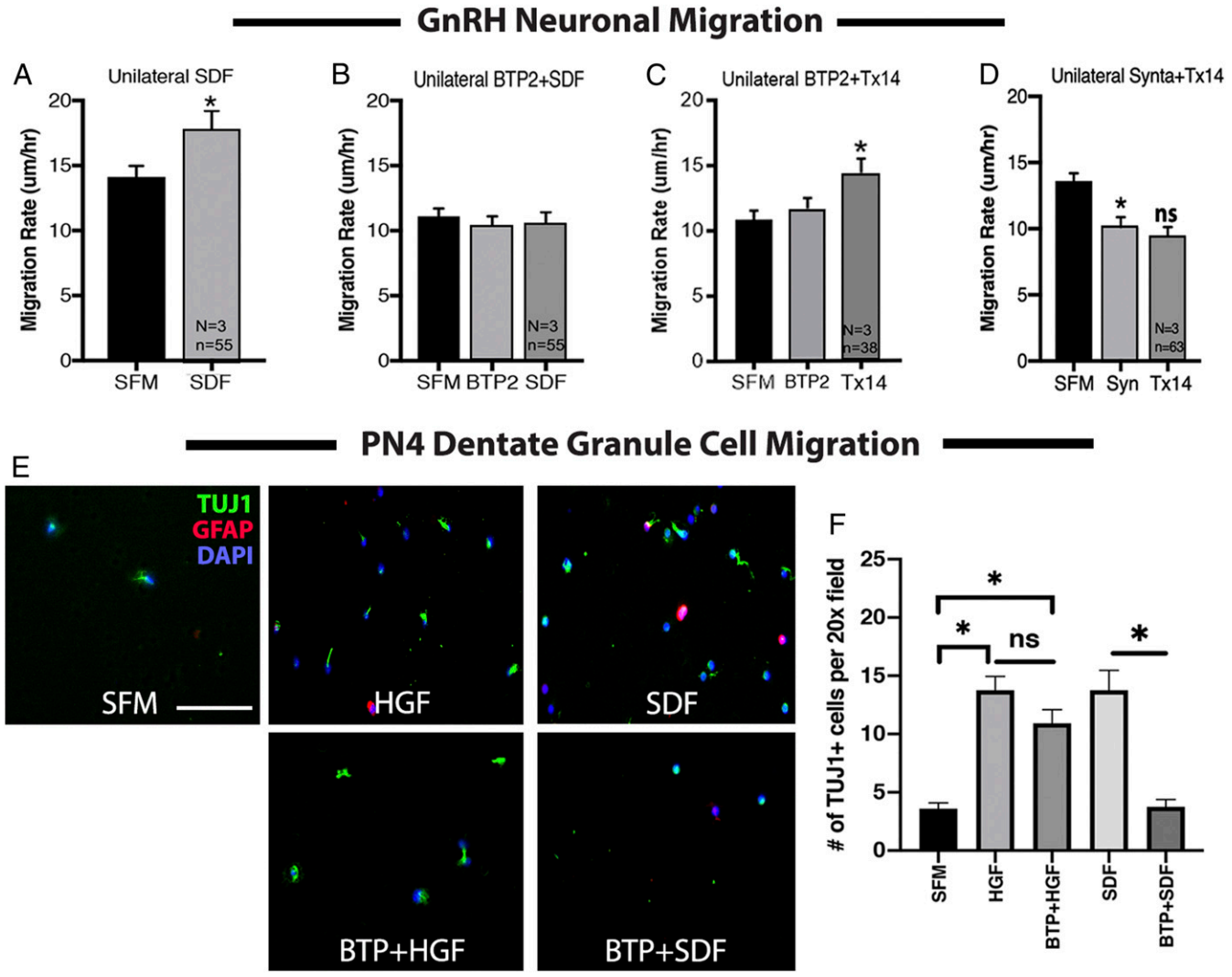

Fig. 5. Specificity of drebrin/CXCR4 interaction. (*A* and *B*) Histograms show that pretreatment of BTP2 (*B*) eliminated the increase in migration rate associated with exogenous application of SDF-1 (*A*, N = 3, $n = 55$, $^*P = 0.0119$; *B*, N = 3, $n = 55$, $P = 0.9445$ [BTP2 to SFM], $P = 0.8782$ [SDF-1 to BTP2], paired *t* test). (*C*) BTP2 application did not block the increase in migration rate associated with activation of GPR37 via TX-14 (N = 3, $n = 38$, $^*P = 0.0041$, paired *t* test). (*D*) In contrast, the CRAC channel blocker, Synta66 (Syn), decreased the GnRH migration rate ($^*P = 0.0001$) and blocked the increase in migration rate normally associated with activation of GPR37 via TX-14 (N = 3, $n = 63$, $P = 0.3973$, paired *t* test). (*E* and *F*) Comparison of DG granule cell response to HGF or SDF in the presence of BTP. DG granule cells showed an increase in migration to both HGF and SDF (*E*, *Top*). BTP treatment blocked the chemokine effect of SDF but had no effect on granule cells exposed to HGF (*E*, *Bottom*). Representative images of each group are shown in *E* (TUJ1, green; GFAP, red; DAPI, blue). Data are shown in histogram (*F*) (unpaired *t* test, N = 3 [pairs of litters], $n = 4$ [20× fields per treatment group/genotype], $^*P < 0.05$, ns, not significant). (Scale bar in *E*, 50 μm.)

binding was predicted at the interface where drebrin's P405, G415, P417, L421, and M422 binds to EB1's T8, F105, N14, W110, and S7, respectively. PRODIGY predicted that EB1 establishes charged–apolar (25%), polar–apolar (25%), and apolar–apolar (15%) bonds with drebrin's PP–BB domains. Additionally, EB1 bound to an artificial drebrin mutant (P405A, G415A, P417A, L421A, and M422A) had an unfavorable binding free energy ($\Delta G_{drebrin(mut)/EB1} = -10.5$ kcal · mol^{-1}) compared to WT drebrin ($\Delta G_{drebrin(wt)/EB1} = -11.2$ kcal · mol^{-1}). To address whether disruption of drebrin affects the anchoring of EB1 to cortical actin regions in migrating neurons, stimulated emission depletion (STED) microscopy was performed to examine changes in EB1/drebrin localization in GnRH cells after application of BTP2 (Fig. 6*B*). In cells not exposed to BTP2, numerous EB1 puncta (1.47/μm) were detected along the drebrin/cortical actin interface. In contrast, significantly fewer EB1 puncta (0.94/μm) were detected along the drebrin/cortical actin interface in cells treated with BTP2 ($P < 0.05$, Fig. 6*C*). Blocking CXCR4 via AMD3100 also caused a decrease in EB1 puncta along the drebrin/cortical actin interface (0.72/μm, $P < 0.05$, Fig. 6 *D* and *E*), indicating proper anchoring of EB1 via drebrin required a functioning SDF-1/CXCR4 pathway. Furthermore, in GnRH neurons derived from *DBN1* KO mice, a similar trend was observed (N = 2, n = 4), with fewer EB1/actin puncta detected compare to the WT group (Fig. 6 *D* and *E*). Notably, the number of EB1/drebrin puncta was similar between control and nocodazole (a microtubule depolymerizing drug)-treated neurons (control = 1.813/μm, Noc = 1.478/μm, $P > 0.05$).

CXCR4 Interacts with Drebrin to Facilitate Neuronal Migration. A model (schematic diagram depicting the interaction between CXCR4, drebrin, actin filaments, EB1, and microtubules

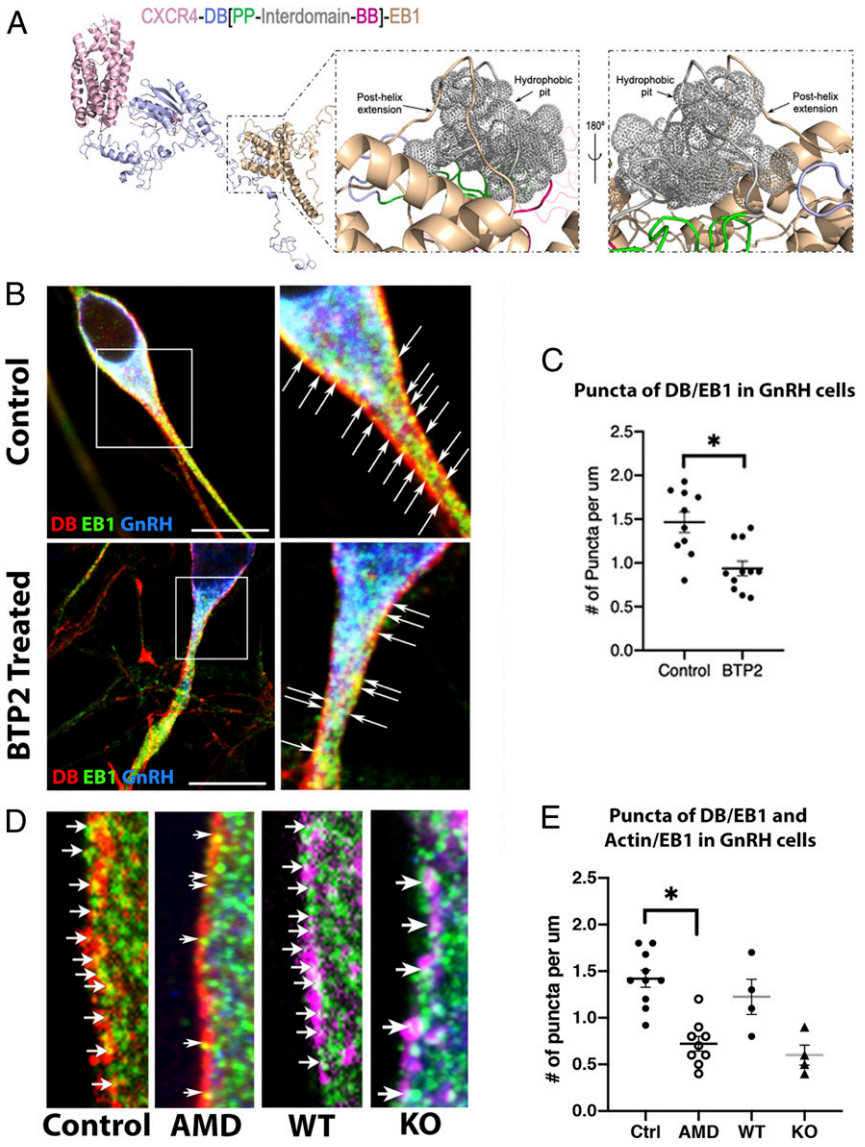

Fig. 6. Drebrin/EB1 interaction in migrating neurons. (*A*) Bioinformatic modeling revealed EB1's posthelix extension latches onto a hydrophobic pit created between drebrin PP and BB domains (residues 404 to 424). (*B* and *C*) BTP treatment decreased DB/EB1 puncta in GnRH cells. Representative STED microscopy images show drebrin (red) and EB1 (green) colocalized in puncta (white arrows) in the leading processes of a GnRH neuron (blue). Higher magnification of boxed images (*Left*) are shown in the right panel. (Scale, 10 μm.) (*C*) Quantification of drebrin/EB1 colocalized puncta in GnRH cells in control and BTP2-treated explants. Significantly less puncta per micrometer were detected in cells from the BTP2-treated group (N = 3, $n = 10$, $^*P < 0.05$, unpaired *t* test). (*D*) Either inhibition of CXCR4 receptor or knockout of drebrin results in decreased EB1 puncta in migrating GnRH neurons. High magnification of representative STED microscopy shows the interactive puncta (white arrows) between drebrin (red) and EB1 (green) in the leading processes of control and AMD3100-treated GnRH neurons (*Left*) and puncta (white arrows) between actin (magenta) and EB1 (green) in GnRH neurons from WT and *DBN1* KO mice (*Right*). (*E*) Quantification of drebrin/EB1 and actin/EB1 in GnRH cells. Less puncta per micrometer were seen in the AMD3100-treated group (unpaired *t* test, N = 3, $n = 9$, $^*P < 0.05$). A similar trend was observed in the *DBN1* KO actin/EB1 puncta compared to the WT control group (N = 2, $n = 4$).

[generated using Biorender, https://biorender.com/]) is shown in Fig. 7. Upon SDF-1 binding to CXCR4, the G protein complex is released from the C terminus of CXCR4, exposing binding epitopes on its ICL1, ICL2, ICL3, and C terminus. CXCR4 then binds with actin-binding protein drebrin, and the latter guides the insertion of microtubule plus ends into cortical actin through interactions with the microtubule plus-end–binding protein EB1. This insertion activates nucleokinesis, promoting neuronal migration.

Discussion

This study investigated how a chemokine receptor, after being activated by its ligand, interacts with cytoskeletal components and promotes neuronal migration. Specifically, we show that after SDF-1 activation, CXCR4 directly interacts with the actin-binding protein drebrin. Drebrin then guides the microtubule plus-end binding protein EB1 to the actin cortex mesh, establishing the dynamic force needed for cell movement. Taken together, these interactions control chemokine-directed cell migration. These results indicate drebrin as a downstream cytoskeletal effector of SDF-1/CXCR4 signaling in developing neurons, connecting cytoskeleton components to extracellular signals that ensure neurons arrive at the correct position to establish appropriate CNS connections.

Bioinformatic modeling predicted binding sites between drebrin and crystallized CXCR4. These predictions were confirmed

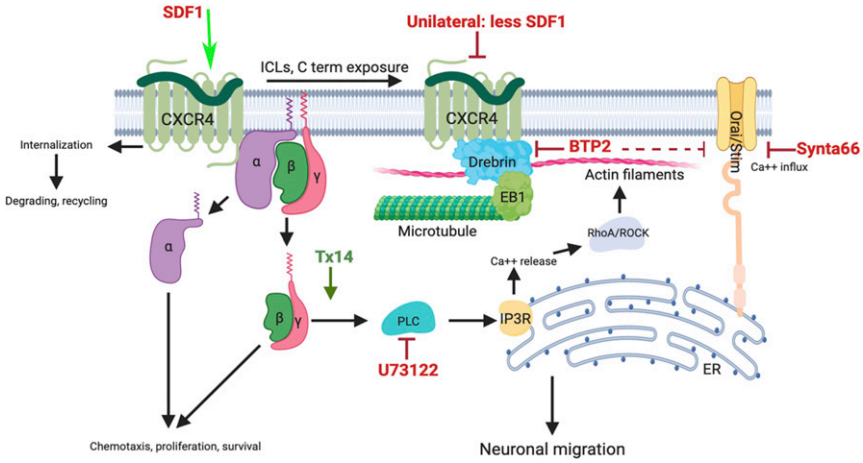

Fig. 7. Schematic diagram of the interaction between CXCR4, drebrin, actin, EB1, and microtubules during SDF-1–induced neuronal migration. Upon SDF-1 binding to CXCR4, the G protein complex is released from the C terminus of CXCR4, exposing drebrin binding sites. CXCR4 then binds with this actin-binding protein, which guides the insertion of microtubule plus-ends into cortical actin via the microtubule plus-end–binding protein EB1. This process then initiates nucleokinesis and subsequently neuronal movement. Inhibition of drebrin (via BTP2) prevents SDF-1 signaling via this pathway and results in slower cell movement. Pharmacological manipulations used in this study are listed in the diagram for reference.

via co-IP. If CXCR4 and drebrin interact during development, one would expect an overlap in phenotypes with either system compromised. Two different point mutations in drebrin have been observed in breast cancer patients (43), but no mutations in drebrin have yet been associated with a neurological disorder, although protein levels are attenuated in patients with Alzheimer's disease, Down syndrome (44), and bipolar disorders (45). At least nine mutations in the *CXCR4* gene have been found to cause Warts, Hypogammaglobulinemia, Immunodeficiency, and Myelokathexis (WHIM) syndrome, a condition characterized by impaired immune function and recurrent bacterial and viral infections. WHIM syndrome is a rare disorder and represents a Mendelian condition caused by a mutation of the CXCR4 gene (heterozygous) and it is a gain of function. Recently, Galli et al. (46) evaluated aspects of neurological function in six WHIM patients and found cerebellar malformation and mild neuromotor and psychopathological dysfunction. Although the data from human patients are limited, using mouse models, one can compare the phenotypes of drebrin and *CXCR4* KOs, with caveats, of course (i.e., deletion of the gene for CXCR4 or SDF-1 results in embryonic/perinatal lethality due to heart failure while *DBN1* KO mice are viable). However, the development of the hippocampus has been examined in both these mutants, while the development of the GnRH system has been examined in *CXCR4* mutants.

In *CXCR4* KO mice, reports indicate that the morphology of the hippocampal DG is dramatically altered (47). Gene expression markers for DG granule neurons and bromodeoxyuridine (BrdU) labeling of dividing cells revealed an underlying defect in the stream of postmitotic cells and secondary DG progenitor cells that migrate toward and form the DG. In the absence of CXCR4, the DG was reduced, and neurons appeared to differentiate prematurely before reaching their target (47). In fact, the migratory stream of homozygote *CXCR4* mutant mice were reported to have a 31% reduction in BrdU-positive cells as compared with WT littermates. Thus, progenitor cells fail to reach the forming DG in sufficient numbers, which remained underpopulated and immature. Our results examining *DBN1* KO mice showed an ∼36% reduction in DG neurons, similar to those reported for *CXCR4* mutants. Furthermore, modified Boyden chamber assays showed that disruption of drebrin impacted the stimulating effect of SDF, but not HGF, on hippocampal granule cell migration, consistent with a specific interaction between drebrin and CXCR4. In addition, we found that in the DG of *DBN1* KO mice, immunostaining for GFAP increased ∼30%. It is known that astrocytes undergo hypertrophic morphological changes coupled with enhanced GFAP expression during astrogliosis associated with cell damage in the brain (48–51). Whether the increase in GFAP was due to an increase in astrocytes and/or astrocytes becoming more GFAP immunoreactive due to astrogliosis remains unclear.

With respect to the GnRH system, *CXCR4* KO mouse embryos had fewer GnRH cells at E13 (reduced 57% compared to controls), with most present in nasal regions (52). In *DBN1* KO mice, we found a 34% reduction in the total number of GnRH cells at E12.5, and as in *CXCR4* mutants, the largest number of cells was detected in nasal regions. Notably, in E14.5 *CXCR4* KO mice, the last stage examined due to embryonic death at E16.5, the total number of GnRH neurons in *CXCR4* KO was still reduced by 48% (16), but the total number was more than that detected at E13 (52). We found that the total number of GnRH neurons in *DBN1* KO mice was similar to control mice by PN4. However, at both PN4 and in adults, the GnRH neurons resided more rostrally in the *DBN1* KO mice, with 55% more GnRH cells present in rostral areas compared to controls. Thus, depletion of drebrin delayed GnRH cell development and decreased GnRH neuronal migration, similar to that reported for the system in the *CXCR4* KO mice.

To directly study the interaction between CXCR4 and drebrin in migrating neurons, we exploited the fact that migration of primary GnRH neurons occurs in nasal explants, and in this system, the level of SDF-1 can be manipulated, both endogenously and exogenously (17). Functional analysis using explants from *DBN1* KO mice and pharmacological manipulations in explants from WT mice confirmed that the SDF-1/CXCR4 pathway that modulates neuronal migration is dependent on drebrin. Morphological analysis of migrating GnRH cells in *DBN1* KO mice and BTP2-treated explants indicated that CXCR4 expression in the leading processes was decreased compared to controls. In addition, computational and morphological analysis was performed on the coupling of the CXCR4/drebrin complex to microtubules via end-binding proteins. Actin-binding proteins guide microtubule plus-ends into cortical actin mesh to generate actin-microtubule contraction, and microtubule insertion at the leading process promotes neuronal migration. (6–8). The mechanism of the drebrin-based actin–microtubule

contact has been shown to require the microtubule plus-end binding protein EB3 (25). In migrating GnRH neurons, the capturing of microtubule plus-ends is via EB1 (31). No structural modeling has been performed on the potential for a drebrin/EB interaction. Thus, we used bioinformatic modeling and found that rapid actin dynamics could be regulated by a direct interaction of the N-terminal domain of actin with drebrin and that insertion of EB1 between the BB and PP domains of drebrin would be stabilized by the hydrophobic pit. These bioinformatic predictions were then confirmed via immunocytochemistry. Using STED microscopy, drebrin was seen robustly expressed along the cortical actin in migrating neurons in control cells, while cells treated with a drebrin inhibitor showed significantly reduced interactive puncta between EB1 and drebrin in the leading process. These data are consistent with drebrin guiding the microtubule plus-ends into the cortical actin to promote neuronal migration. Consistent with this, EB1 was less expressed in migrating cells in *DBN1* KO mice (*SI Appendix*, Fig. S4). Notably, the expression pattern of drebrin did not appear to change after pharmacological inhibition (Fig. 4), suggesting that drebrin maintained its association with actin helices along the cortical actin mesh. Characterization of the action of BTP2 on drebrin may provide a better understanding of the mechanisms involved in drebrin/actin binding. Phosphorylation of S142 in drebrin has been shown to be important for coupling actin helices, followed by EB3 insertion between the BB and PP domain (53). Whether these sites remain essential when CXCR4 is bound to drebrin remains to be investigated.

To our knowledge, no previous study has reported a protein, outside F-actin and EBs, that has been identified to bind to embryonic drebrin (drebrin E) in migrating neurons. In astrocytes, drebrin E was shown to link connexin 43 (Cx43) and the cytoplasmic actin mesh at gap junctions (54–56). Depletion of drebrin with small interfering RNA (siRNA) resulted in impaired cell–cell coupling, internalization of gap junctions, and targeting of Cx43 to a degradative pathway (54). Enhanced astrogliosis has been reported in mice in which Cx43 was depleted in astrocytes (51). Thus, the increase in GFAP reactivity (a sign of astrogliosis) seen in the *DBN1* KO hippocampus in our study may be due to decreased Cx43 in this cell subtype. Several scaffolding proteins have been reported to directly bind to the adult form of drebrin (drebrin A) and influence its binding to actin in dendritic spines, including profilin (57), mDia2 formin (58), and homer2 (27, 59, 60). An interaction was also reported for the transcriptional regulator Spikar (spine and karyoplasm protein, gene name ZMYDN8) and drebrin in the dendritic spines of rat hippocampal neurons (26, 61).

Drebrin A (706 amino acid [aa] length) differs from E (660 aa length) in that it contains a neuron-specific Ins2 insert (46 amino acids) prior to the start of its C-terminal PP domain (62, 63). However, no clear functional differences have been described between these two isoforms. Studies have shown that proteins associated with dendritic spines bind to drebrin A at different regions: profilin at the C-terminal PP domain (57), formin in an unspecified region that spans residues 300 to 700 (58), Spikar/ZMYDN8 at the N-terminal ADFH domain (residues ~1 to 135), and Homer 2/cupidin using a conserved type-1 homer binding motif (HBM1) that lies within the C-terminal BB domains (27, 60). Multiple studies have shown that drebrin E uses its N terminus to bind to Cx43 (54, 56) and its C terminus to bind to EB3 (53, 62). In T cells, drebrin E binds to CXCR4 (18) using the highly ordered N-terminal ADFH, CC, and Hel domains (residues 1 to 366). In the present study, bioinformatic prediction supports drebrin E binding to CXCR4 using its N-terminal ADFH, CC, and Hel domains (residues 90 to 290), and EB1, the paralog of EB3, with its C-terminal PP and BB domains (residues 404 to 424) in migrating neurons. Clearly, drebrin is a large, flexible intracellular protein with evolutionarily conserved structural domains in vertebrates. These protein domains give drebrin the ability to bind to a wide variety of molecules, accessory or effector proteins that can then be linked to cytoskeletal changes.

In sum, using different developing CNS systems, we show a mechanism whereby drebrin acts as an important connector between chemokine signals and actin/microtubule dynamics during neuronal migration. Specifically, we show that CXCR4, upon activation by its ligand SDF-1, binds directly with drebrin at the cortical actin mesh and drebrin via end-binding protein EB1 to microtubules. This mechanism brings insight into how an extracellular signal can convert into an intracellular force via direct binding and facilitate cellular movement.

Materials and Methods

Animals. Mouse lines used in this study: NIH Swiss and *DBN1* KO mice (Dr. Avery August, Cornell University). All procedures were performed in accordance with National Institute of Neurological Disorders and Stroke (NINDS) ACUC animal ethics guidelines. E12.5 NIH Swiss, E12.5 WT, and *DBN1* KO mouse littermates were isolated from timed-mated Swiss or *DBN1* heterozygous females, washed in phosphate-buffered saline (PBS), and fixed in 4% formaldehyde (1 h), then transferred into 30% sucrose (4 °C overnight). Embryos were then rinsed with PBS, embedded in O.C.T. compound (Thermo Fisher) and stored at −80 °C until sectioning. Serial sections (14 μm, parasagittal plane) were cut on a Leica CM3050 cryostat and mounted onto SuperFrost-charged slides (Daigger) and stored at −80 °C until immunostaining. PN4 and adult (>PN45) WT and *DBN1* KO animals were euthanized, brains were removed, postfixed, cryoprotected, embedded in O.C.T compound, and frozen and stored at −80 °C. Another group of adult WT and *DBN1* KO animals were perfused, brains were removed, postfixed, cryoprotected, embedded in O.C.T compound, and frozen and stored at −80 °C. PN4 and adult brains were coronally cryosectioned (20 μm) into series and stored at −80 °C until use. WT and *DBN1* KO PN4 DG were collected and lysed for modified Boyden chamber assays. Explants were generated as previously described (34, 64). Briefly, timed-mated NIH Swiss or *DBN1* heterozygous female mice were euthanized and E11.5 embryos collected. Nasal pit(s) with or without nasal midline cartilage were isolated and cultured at 37 °C with 5% CO_2 in SFM (34). At 3 d in vitro (DIV), the explants were treated with SFM containing fluorodeoxyuridine (FUDR, Sigma, 8×10^{-5} M) to inhibit mitosis of nonneural tissue (fibroblasts, etc.). Explants at 4DIV were either used for migration assays or STED puncta analysis or fixed in 4% formaldehyde for further immunostaining.

Immunocytochemistry. Primary antibodies used were: rabbit polyclonal anti-GnRH [SW-1, 1:5,000 for explants, 1:15,000 in vivo, (65)], mouse monoclonal anti-GnRH/SMI (FID3C5, Dr. Karande, 1:4,000), chicken anti-GnRH (Aves, 1:100), rabbit polyclonal anti-drebrin (Abcam, 1:800), goat polyclonal anti-CXCR4 N terminus (Abcam, 1:1,000), rat anti-EB1 (Abcam, 1:750), biotin conjugated NeuN (Chemicon, 1:500), rabbit polyclonal anti-GFAP (Immunostar, 1:9), rabbit polyclonal anti-Sox2 (Chemicon, 1:1,000), and chicken anti-beta-tubulin III (Aves, 1:700). Tissue from *DBN1* KO mice was used to verify the specificity of the drebrin antibody (*SI Appendix*, Fig. S5). In mammals, two drebrin isoforms have been identified: drebrin A and drebrin E (66). The drebrin antibody listed above recognizes both forms. However, in adult neurons, drebrin A is primarily localized at dendritic spines, whereas drebrin E is localized in developing tissue around the cell body and leading processes of migrating cells (67, 68). Explants, GnRH cells, or mouse tissue sections were stained using either immunofluorescence or chromogens (*SI Appendix, Supplemental Methods*). Pictures were taken using Nikon Eclipse E800 upright microscope for chromogen staining. Fluorescent images were taken on a Nikon Eclipse TE200 spinning disk microscope (Yogawa, Nikon) equipped with an EMCCD ImageM digital camera (Hamamatsu) with iVision software (BioVision) or a Leica STED 3X microscope (NINDS imaging facility). Images were further processed/analyzed using NIH ImageJ software (W. Rasband, NIH, Bethesda).

Co-IP and Western Blot. Primary antibodies used in co-IP and Western blot were as follows: rabbit anti-drebrin (Abcam, 20 μg/mL on beads), goat anti-CXCR4 (Abcam, 20 μg/mL on beads), mouse anti-drebin (Abcam, 1:1,000 on blot), chicken anti-CXCR4 (Sigma, 1:2,000 on blot), rabbit anti-CCKA (Incstar, 1:1,000 on blot), and goat anti-GAPDH (Sigma, 1:2,000 on blot). Refer to *SI Appendix, Supplemental Methods* for detailed procedures.

Analysis of GnRH Neurons and Hippocampi in WT and *DBN1* KO Animals. The total number and distribution of immunostained GnRH neurons in E12.5, PN4, and adult brains were analyzed. Anatomical regions for GnRH distribution were determined by animal age—E12.5: nose (N), nasal forebrain junction, and brain; PN4 and Adult: anterior to OVLT, OVLT region, and caudal to OVLT. Cell bodies were counted using a bright-field microscope (Nikon E800) and results compared using Prism (total cell number, unpaired *t* test, $P < 0.05$ and cell distribution χ^2, $P < 0.001$). NeuN (neurons)- and GFAP (astrocytes)-immunostained PN4 and adult hippocampi were imaged and exported into ImageJ for analysis. Relative density of NeuN or GFAP immunostaining within the DG was measured and compared using Prism (unpaired *t* test, $P < 0.05$). Sox2-positive cells were counted and plotted between WT and KO animals.

Modified Boyden Chamber Assays. The DG was dissected from both WT and *DBN1* KO PN4 animals. Suspension of DG granule cells were obtained by papain treatment (Worthington) for 40 min at 37 °C and with continuous shaking. Briefly, collected DG were cut into small pieces, incubated with papain solution with DNase, and triturated via fetal bovine serum (FBS)-coated 1,000-μL pipette. Cell mixture was separated via a 65 to 35% Percoll gradient (Sigma) to rid interneurons, glial cells, epithelial cells, and red blood cells. Final suspension contained at least 70% DG granule cells. Modified Boyden chambers (Transwell inserts, Falcon) with 8-μm pores were placed in a standard 24-well plate (Falcon), coated with Poly-L-Lysine (Invitrogen) for 10 min at room temperature and rinsed with dH_2O. Granule cells (2×10^5) in Neurobasal media (Invitrogen) supplemented with B27 (Gibco) and Glutamax (Invitrogen) were added to the top chambers. Media containing different attractants (HGF: 25 ng/mL, Sigma; SDF-1: 5 μg/mL, Sigma) were placed in the bottom chambers. To block drebrin, BTP2 (5 μM, Millipore) was placed in both top and bottom chambers. The final volume was as follows: top chamber, 200 μL and bottom chamber, 800 μL. Plates were placed in a humidified incubator with 5% CO_2 at 37 °C for 24 h. After incubation period, Transwell inserts were washed, and the upper chamber cells were gently removed via a damp cotton swab. The membranes were separated from the chamber, fixed in 4% formaldehyde, and processed for immunofluorescent staining. Pictures were taken on a Nikon Eclipse E800 upright microscope with a 20× objective, and TUJ1-positive cells were counted using ImageJ and compared between groups using Prism software.

Migration Assays. Drugs used in migration assays were as follows: BTP2 (Drebrin blocker, Millipore, 5 μM), SDF-1 (CXCR4 ligand, Sigma, 5 μg/mL), PIC (antagonist of $GABA_AR$, Tocris, 0.1 mM), TX-14A (GPR37 agonist, Tocris, 1 μM), U73122 (PLC blocker, Enzo Life Sciences, 2.5 μM), and Synta66 (CRAC channel blocker, Sigma, 10 μM). Migration assays were performed on an inverted Nikon TE 2000 microscope (extra-long working distance 20× objective) equipped with differential interference contrast (DIC) optics, a z-stage (Ludl), and an ICCD camera (Retiga). Explants were placed in a chamber (5% CO_2, 37 °C, Live cell, Pathology Devices, Inc). Movement of GnRH cells from NIH swiss mice was monitored for 2 or 3 h, with treatment periods being for 1 h each, with the first 1 h being the control period (SFM only). Movement of GnRH cells from WT and *DBN1* KO littermates was monitored for a single 1 h SFM period only. Five z-stage images (5 μm apart) were taken every 1 min for 60 min and were compiled into a movie. Linear distance was calculated from the x and y coordinates of each cell between the first and last frame and migration rate for each 1 h period calculated as the distance traveled over time (micrometers per hour).

EB1 Insertion Puncta Analysis. Control, BTP2-treated, and AMD3100 (Sigma, 25 μg/mL)-treated, as well as explants from *DBN1* KO mice were immunofluorescently stained for GnRH, EB1, drebrin (WT), or phalloidin conjugated with Alexa 555 (Invitrogen, explants derived from *DBN1* KO mice). Images were acquired via STED microscopy. For GnRH (405 nm), a 442 nm depletion laser was used; for EB1 (488 nm), a 592-nm depletion laser was used; for drebrin or phalloidin (555 nm), a 660-nm depletion laser was used. Images were imported into ImageJ, and each cell's nuclear center was determined. From the cell center, a 10-μm area toward the leading process was drawn, and colocalized puncta between EB1 and drebrin or EB1 and phalloidin were counted within this area. The total number of puncta in control and treated groups were analyzed using unpaired *t* test, $P < 0.05$. Nocodazole (microtubule polymerization inhibitor, Sigma, 1 μM) treated explants were also stained for GnRH, EB1, and drebrin and EB1/drebrin puncta plotted.

Structural Modeling. CXCR4 structure was extracted directly from its resolved crystal (Protein Data Bank: 3ODU). Drebrin E and EB1 structures were generated using I-TASSER (69, 70) from their FASTA sequences and resolved using PyMOL v2.3.2 molecular graphics software. Docking of crystallized CXCR4/drebrin and drebrin/EB1 were generated by SwarmDock (71) and confirmed by PatchDock (72). Residues predicted to interact at the interface were predicted by PIMA (73) and PRODIGY (74). Refer to *SI Appendix, Supplemental Methods* for detailed procedures.

Statistics.

In vivo statistics. For each age point, at least $n = 3$ WT/KO littermate-paired animals were stained and GnRH cells counted. Student's unpaired *t* test was used to compare the GnRH numbers, and χ^2 analysis was performed to examine the distribution of cells between genotypes. Subsequent unpaired *t* tests identified regions with the greatest difference. For hippocampal analysis, three representative NeuN-, GFAP-, or Sox2-stained sections were selected from each animal (n = at least 3 animals/genotype). For NeuN, three regions of interest were imaged on each section and density readings obtained. For GFAP, the entire DG was imaged and density readings obtained. Density readings were analyzed using Student's unpaired *t* test in Prism 8. For Sox2, numbers of Sox2 positive cells along SGZ were counted and compared (unpaired *t* test) in Prism.

In vitro statistics. For migration assays, at least three explants (N) and 35 cells (n) were used for each treatment group and a paired Student's *t* test (same cell recorded and analyzed pre- and posttreatment, $P < 0.05$) performed on migration rates. From previous work (17), cells with migration rates above 22.23 μm/h and below 3.83 μm/h during the SFM period were omitted due to probability of reversing speed independent of treatment. For STED puncta analysis, at least 10 cells from 3 explants (3 to 4 cells/explant) were imaged, except for actin/EB1 localization in GnRH cells from *DBN1* KO mice where N = 2, and statistics were not performed (Fig. 6*E*). Comparison of control and treated groups in all other experiments was performed via unpaired *t* test, $P < 0.05$. For modified Boyden chamber assays, seven animals per group were collected, cells mixed and plated, and experimental groups designated. This procedure was repeated three times (N) for each experiment. After staining, four 20× views were randomly selected on the stained polycarbonate membrane and pictures taken. The average cell numbers within each group were calculated and compared via Student's unpaired *t* test ($P < 0.05$).

Data Availability. All study data are included in the article and *SI Appendix*.

ACKNOWLEDGMENTS. This work was supported by the Intramural Research Program of the National Institutes of Health, National Institute of Neurological Disorders and Stroke (Grant ZIA-NS-002824). We thank Dr. Avery August for providing *DBN1* KO animals, NINDS core imaging facility, and Dr. Carolyn Smith for assisting with STED microscopy, Ms. Katherine Pizano (Postbaccalaureate fellow, cellular and developmental neurobiology section [CDNS]) for animal perfusion; Dr. Aybike Saglam (Postdoctoral fellow, CDNS) for aiding with PN4 hippocampi isolation and sharing primary culture protocol; Ms. Cassandra Rios (Postbaccalaureate fellow, CDNS), Ms. Zaria Wilson (Newcomb fellow, NIH), and Ms. Aracely Barajas (Summer student, NIH) for cryosectioning; and Dr. Stephanie Constantin (Scientist, CDNS) and Mr. Dakota Jacobs (Postbaccalaureate fellow, CDNS) for their valuable comments on the manuscript.

1. P. Rakic, Principles of neural cell migration. *Experientia* **46**, 882–891 (1990).
2. Q. Ma *et al*., Impaired B-lymphopoiesis, myelopoiesis, and derailed cerebellar neuron migration in CXCR4- and SDF-1-deficient mice. *Proc. Natl. Acad. Sci. U.S.A.* **95**, 9448–9453 (1998).
3. Y. R. Zou, A. H. Kottmann, M. Kuroda, I. Taniuchi, D. R. Littman, Function of the chemokine receptor CXCR4 in haematopoiesis and in cerebellar development. *Nature* **393**, 595–599 (1998).
4. R. K. Stumm *et al*., CXCR4 regulates interneuron migration in the developing neocortex. *J. Neurosci.* **23**, 5123–5130 (2003).
5. S. Wray, Development of gonadotropin-releasing hormone-1 neurons. *Front. Neuroendocrinol.* **23**, 292–316 (2002).
6. T. D. Pollard, G. G. Borisy, Cellular motility driven by assembly and disassembly of actin filaments. *Cell* **112**, 453–465 (2003).
7. I. M. Tolić-Nørrelykke, Force and length regulation in the microtubule cytoskeleton: Lessons from fission yeast. *Curr. Opin. Cell Biol.* **22**, 21–28 (2010).
8. D. E. Lysko, M. Putt, J. A. Golden, SDF1 reduces interneuron leading process branching through dual regulation of actin and microtubules. *J. Neurosci.* **34**, 4941–4962 (2014).
9. A. Bagri *et al*., The chemokine SDF1 regulates migration of dentate granule cells. *Development* **129**, 4249–4260 (2002).
10. I. Marchionni *et al*., Distinctive properties of CXC chemokine receptor 4-expressing Cajal-Retzius cells versus GABAergic interneurons of the postnatal hippocampus. *J. Physiol.* **588**, 2859–2878 (2010).

11. G. Li *et al*., Regional distribution of cortical interneurons and development of inhibitory tone are regulated by Cxcl12/Cxcr4 signaling. *J. Neurosci.* **28**, 1085–1098 (2008).
12. Y. Zhu *et al*., Role of the chemokine SDF-1 as the meningeal attractant for embryonic cerebellar neurons. *Nat. Neurosci.* **5**, 719–720 (2002).
13. K. Hagihara *et al*., Shp2 acts downstream of SDF-1alpha/CXCR4 in guiding granule cell migration during cerebellar development. *Dev. Biol.* **334**, 276–284 (2009).
14. G. J. Huang *et al*., Ectopic cerebellar cell migration causes maldevelopment of Purkinje cells and abnormal motor behaviour in Cxcr4 null mice. *PLoS One* **9**, e86471 (2014).
15. S. A. Tobet, G. A. Schwarting, Minireview: Recent progress in gonadotropin-releasing hormone neuronal migration. *Endocrinology* **147**, 1159–1165 (2006).
16. Y. Toba, J. D. Tiong, Q. Ma, S. Wray, CXCR4/SDF-1 system modulates development of GnRH-1 neurons and the olfactory system. *Dev. Neurobiol.* **68**, 487–503 (2008).
17. F. Casoni *et al*., SDF and GABA interact to regulate axophilic migration of GnRH neurons. *J. Cell Sci.* **125**, 5015–5025 (2012).
18. M. Pérez-Martínez *et al*., F-actin-binding protein drebrin regulates CXCR4 recruitment to the immune synapse. *J. Cell Sci.* **123**, 1160–1170 (2010).
19. X. P. Dun *et al*., Drebrin controls neuronal migration through the formation and alignment of the leading process. *Mol. Cell. Neurosci.* **49**, 341–350 (2012).
20. M. Sonego *et al*., Drebrin regulates neuroblast migration in the postnatal mammalian brain. *PLoS One* **10**, e0126478 (2015).
21. N. Trivedi *et al*., Drebrin-mediated microtubule-actomyosin coupling steers cerebellar granule neuron nucleokinesis and migration pathway selection. *Nat. Commun.* **8**, 14484 (2017).
22. K. Hayashi, K. Kubo, A. Kitazawa, K. Nakajima, Cellular dynamics of neuronal migration in the hippocampus. *Front. Neurosci.* **9**, 135 (2015).
23. Y. Mimura-Yamamoto *et al*., Dynamics and function of CXCR4 in formation of the granule cell layer during hippocampal development. *Sci. Rep.* **7**, 5647 (2017).
24. J. C. Edmondson, M. E. Hatten, Glial-guided granule neuron migration in vitro: A high-resolution time-lapse video microscopic study. *J. Neurosci.* **7**, 1928–1934 (1987).
25. S. Geraldo, U. K. Khanzada, M. Parsons, J. K. Chilton, P. R. Gordon-Weeks, Targeting of the F-actin-binding protein drebrin by the microtubule plus-tip protein EB3 is required for neuritogenesis. *Nat. Cell Biol.* **10**, 1181–1189 (2008).
26. N. Yao *et al*., The structure of the ZMYND8/drebrin complex suggests a cytoplasmic sequestering mechanism of ZMYND8 by drebrin. *Structure* **25**, 1657–1666.e3 (2017).
27. Z. Li *et al*., Homer tetramer promotes actin bundling activity of drebrin. *Structure* **27**, 27–38.e4 (2019).
28. P. Giacobini *et al*., Cholecystokinin modulates migration of gonadotropin-releasing hormone-1 neurons. *J. Neurosci.* **24**, 4737–4748 (2004).
29. S. Wray, A. Nieburgs, S. Elkabes, Spatiotemporal cell expression of luteinizing hormone-releasing hormone in the prenatal mouse: Evidence for an embryonic origin in the olfactory placode. *Brain Res. Dev. Brain Res.* **46**, 309–318 (1989).
30. D. J. Solecki *et al*., Myosin II motors and F-actin dynamics drive the coordinated movement of the centrosome and soma during CNS glial-guided neuronal migration. *Neuron* **63**, 63–80 (2009).
31. B. I. Hutchins, S. Wray, Capture of microtubule plus-ends at the actin cortex promotes axophilic neuronal migration by enhancing microtubule tension in the leading process. *Front. Cell. Neurosci.* **8**, 400 (2014).
32. O. Berger, G. Li, S. M. Han, M. Paredes, S. J. Pleasure, Expression of SDF-1 and CXCR4 during reorganization of the postnatal dentate gyrus. *Dev. Neurosci.* **29**, 48–58 (2007).
33. G. L. Ming, H. Song, Adult neurogenesis in the mammalian brain: Significant answers and significant questions. *Neuron* **70**, 687–702 (2011).
34. S. Fueshko, S. Wray, LHRH cells migrate on peripherin fibers in embryonic olfactory explant cultures: An in vitro model for neurophilic neuronal migration. *Dev. Biol.* **166**, 331–348 (1994).
35. C. Tian, L. Du, Y. Zhou, M. Li, Store-operated CRAC channel inhibitors: Opportunities and challenges. *Future Med. Chem.* **8**, 817–832 (2016).
36. J. C. Mercer *et al*., Chemico-genetic identification of drebrin as a regulator of calcium responses. *Int. J. Biochem. Cell Biol.* **42**, 337–345 (2010).
37. S. W. Ng, J. di Capite, K. Singaravelu, A. B. Parekh, Sustained activation of the tyrosine kinase Syk by antigen in mast cells requires local Ca2+ influx through Ca2+ release-activated Ca2+ channels. *J. Biol. Chem.* **283**, 31348–31355 (2008).
38. H. Saadi, Y. Shan, D. Marazziti, S. Wray, GPR37 signaling modulates migration of olfactory ensheathing cells and gonadotropin releasing hormone cells in mice. *Front. Cell. Neurosci.* **13**, 200 (2019).
39. S. Herlitze *et al*., Modulation of Ca2+ channels by G-protein beta gamma subunits. *Nature* **380**, 258–262 (1996).
40. X. Zhang, M. Gueguinou, M. Trebak, "Store-independent orai channels regulated by STIM" in *Calcium Entry Channels in Non-Excitable Cells*, J. A. Kozak, J. W., Putney Jr, Eds. (Boca Raton, FL, 2018), pp. 197–214, 10.1201/9781315152592-11.
41. R. C. Meyer, M. M. Giddens, S. A. Schaefer, R. A. Hall, GPR37 and GPR37L1 are receptors for the neuroprotective and glioprotective factors prosaptide and prosaposin. *Proc. Natl. Acad. Sci. U.S.A.* **110**, 9529–9534 (2013).
42. Y. Wen *et al*., EB1 and APC bind to mDia to stabilize microtubules downstream of Rho and promote cell migration. *Nat. Cell Biol.* **6**, 820–830 (2004).
43. T. Sjöblom *et al*., The consensus coding sequences of human breast and colorectal cancers. *Science* **314**, 268–274 (2006).
44. H. W. Kim, S. I. Rapoport, J. S. Rao, Altered expression of apoptotic factors and synaptic markers in postmortem brain from bipolar disorder patients. *Neurobiol. Dis.* **37**, 596–603 (2010).
45. K. S. Shim, G. Lubec, Drebrin, a dendritic spine protein, is manifold decreased in brains of patients with Alzheimer's disease and Down syndrome. *Neurosci. Lett.* **324**, 209–212 (2002).
46. J. Galli *et al*., Cerebellar involvement in warts hypogammaglobulinemia immunodeficiency myelokathexis patients: Neuroimaging and clinical findings. *Orphanet J. Rare Dis.* **14**, 61 (2019).
47. M. Lu, E. A. Grove, R. J. Miller, Abnormal development of the hippocampal dentate gyrus in mice lacking the CXCR4 chemokine receptor. *Proc. Natl. Acad. Sci. U.S.A.* **99**, 7090–7095 (2002).
48. H. Chen *et al*., Regional and developmental variations of GFAP and actin mRNA levels in the CNS of jimpy and shiverer mutant mice. *J. Mol. Neurosci.* **4**, 89–96 (1993).
49. L. F. Eng, R. S. Ghirnikar, GFAP and astrogliosis. *Brain Pathol.* **4**, 229–237 (1994).
50. R. G. Nagele *et al*., Contribution of glial cells to the development of amyloid plaques in Alzheimer's disease. *Neurobiol. Aging* **25**, 663–674 (2004).
51. N. Theodoric, J. F. Bechberger, C. C. Naus, W. C. Sin, Role of gap junction protein connexin43 in astrogliosis induced by brain injury. *PLoS One* **7**, e47311 (2012).
52. G. A. Schwarting, T. R. Henion, J. D. Nugent, B. Caplan, S. Tobet, Stromal cell-derived factor-1 (chemokine C-X-C motif ligand 12) and chemokine C-X-C motif receptor 4 are required for migration of gonadotropin-releasing hormone neurons to the forebrain. *J. Neurosci.* **26**, 6834–6840 (2006).
53. D. C. Worth, C. N. Daly, S. Geraldo, F. Oozeer, P. R. Gordon-Weeks, Drebrin contains a cryptic F-actin-bundling activity regulated by Cdk5 phosphorylation. *J. Cell Biol.* **202**, 793–806 (2013).
54. E. Butkevich *et al*., Drebrin is a novel connexin-43 binding partner that links gap junctions to the submembrane cytoskeleton. *Curr. Biol.* **14**, 650–658 (2004).
55. C. Stout, D. A. Goodenough, D. L. Paul, Connexins: Functions without junctions. *Curr. Opin. Cell Biol.* **16**, 507–512 (2004).
56. C. Ambrosi *et al*., Connexin43 forms supramolecular complexes through non-overlapping binding sites for drebrin, tubulin, and ZO-1. *PLoS One* **11**, e0157073 (2016).
57. A. Mammoto *et al*., Interactions of drebrin and gephyrin with profilin. *Biochem. Biophys. Res. Commun.* **243**, 86–89 (1998).
58. A. A. Ginosyan, E. E. Grintsevich, E. Reisler, Neuronal drebrin A directly interacts with mDia2 formin to inhibit actin assembly. *Mol. Biol. Cell* **30**, 646–657 (2019).
59. J. A. Stiber *et al*., Homer modulates NFAT-dependent signaling during muscle differentiation. *Dev. Biol.* **287**, 213–224 (2005).
60. Y. Shiraishi-Yamaguchi *et al*., Interaction of Cupidin/Homer2 with two actin cytoskeletal regulators, Cdc42 small GTPase and Drebrin, in dendritic spines. *BMC Neurosci.* **10**, 25 (2009).
61. H. Yamazaki *et al*., Spikar, a novel drebrin-binding protein, regulates the formation and stabilization of dendritic spines. *J. Neurochem.* **128**, 507–522 (2014).
62. T. Shirao *et al*., The role of drebrin in neurons. *J. Neurochem.* **141**, 819–834 (2017).
63. K. Hanamura, Y. Kamata, H. Yamazaki, N. Kojima, T. Shirao, Isoform-dependent regulation of drebrin dynamics in dendritic spines. *Neuroscience* **379**, 67–76 (2018).
64. U. Klenke, C. Taylor-Burds, Culturing embryonic nasal explants for developmental and physiological study. *Curr. Protoc. Neurosci.* **Chapter 3**, 3 25 21–3 25 16 (2012).
65. S. Wray, B. H. Gähwiler, H. Gainer, Slice cultures of LHRH neurons in the presence and absence of brainstem and pituitary. *Peptides* **9**, 1151–1175 (1988).
66. N. Kojima, Y. Kato, T. Shirao, K. Obata, Nucleotide sequences of two embryonic drebrins, developmentally regulated brain proteins, and developmental change in their mRNAs. *Brain Res.* **464**, 207–215 (1988).
67. T. Mizui *et al*., Drebrin E is involved in the regulation of axonal growth through actin-myosin interactions. *J. Neurochem.* **109**, 611–622 (2009).
68. N. Koganezawa, K. Hanamura, Y. Sekino, T. Shirao, The role of drebrin in dendritic spines. *Mol. Cell. Neurosci.* **84**, 85–92 (2017).
69. J. Yang, Y. Zhang, I-TASSER server: New development for protein structure and function predictions. *Nucleic Acids Res.* **43**, W174–W181 (2015).
70. C. Zhang, P. L. Freddolino, Y. Zhang, COFACTOR: Improved protein function prediction by combining structure, sequence and protein-protein interaction information. *Nucleic Acids Res.* **45**, W291–W299 (2017).
71. M. Torchala, I. H. Moal, R. A. Chaleil, J. Fernandez-Recio, P. A. Bates, SwarmDock: A server for flexible protein-protein docking. *Bioinformatics* **29**, 807–809 (2013).
72. D. Schneidman-Duhovny, Y. Inbar, R. Nussinov, H. J. Wolfson, PatchDock and SymmDock: Servers for rigid and symmetric docking. *Nucleic Acids Res.* **33**, W363–W367 (2005).
73. O. K. Mathew, R. Sowdhamini, PIMADb: A database of protein-protein interactions in huge macromolecular assemblies. *Bioinform. Biol. Insights* **10**, 105–109 (2016).
74. L. C. Xue, J. P. Rodrigues, P. L. Kastritis, A. M. Bonvin, A. Vangone, PRODIGY: A web server for predicting the binding affinity of protein-protein complexes. *Bioinformatics* **32**, 3676–3678 (2016).